Kidney International, Vol. 51 (1997), pp. 125–137

Regulation of AE1 anion exchanger and H^+-ATPase in rat cortex by acute metabolic acidosis and alkalosis

IVAN SABOLIĆ, DENNIS BROWN, STEPHEN L. GLUCK, and SETH L. ALPER

Institute for Medical Research and Occupational Health, Zagreb, Croatia, Renal Unit, Massachusetts General Hospital, Molecular Medicine and Renal Units, Beth Israel Hospital, Departments of Pathology, Cell Biology, and Medicine, Harvard Medical School, Boston, Massachusetts; and Departments of Cell Biology and Medicine, Washington University School of Medicine, St. Louis, Missouri, USA

Regulation of AE1 anion exchanger and H^+-ATPase in rat cortex by acute metabolic acidosis and alkalosis. The cortical collecting duct (CCD) mediates net secretion or reabsorption of protons according to systemic acid/base status. Using indirect immunofluorescence, we examined the localization and abundance of the vacuolar H^+-ATPase and the AE1 anion exchanger in intercalated cells (IC) of rat kidney connecting segment (CNT) and CCD during acute (6 hr) metabolic (NH_4Cl) acidosis and respiratory ($NaHCO_3$) alkalosis. AE1 immunostaining intensity quantified by confocal microscopy was elevated in metabolic acidosis and substantially reduced in metabolic alkalosis. AE1 immunostaining was restricted to Type A IC in all conditions, and the fraction of $AE1^+$ IC was unchanged in CNT and CCD. Metabolic acidosis was accompanied by redistribution of H^+-ATPase immunostaining towards the apical surface of IC, and metabolic alkalosis was accompanied by H^+-ATPase redistribution towards the basal surface of IC. Therefore, acute metabolic acidosis produced changes consistent with increased activity of Type A IC and decreased activity of Type B IC, whereas acute metabolic alkalosis produced changes corresponding to increased activity of Type B IC and decreased activity of Type A IC. These data demonstrate that acute systemic acidosis and alkalosis modulate the cellular distribution of two key transporters involved in proton secretion in the distal nephron.

Intercalated cells (IC) of the mammalian kidney are highly specialized epithelial cells involved in acid-base transport. Functionally, at least two types of IC mediate acid secretion and base secretion in the connecting segment and collecting ducts, the A-type and B-type IC, respectively [reviewed in 1]. These transport functions are thought to be mediated by the coordinated activities of a vacuolar-type H^+-ATPase and a Cl^-/HCO_3^- exchanger at opposite IC surface membranes, as demonstrated by immunolocalization of these key proteins [2–7] and by fluorometric measurement of pH_i in single cells of isolated perfused tubules [8–10]. B-type (or other) IC have also been proposed to serve as transcellular pathways for reabsorption of K^+ and Cl^-, via the activities of an H^+/K^+ ATPase and a Cl^-/HCO_3^- exchanger at the apical surface [1, 11].

Though the molecular identity of the apical Cl^-/HCO_3^- exchanger(s) remains the subject of debate [12–14], many immunocytochemical studies have demonstrated AE1 immunoreactivity at the basolateral surface of the type A, acid-secreting IC [2–4, 6, 7, 15]. AE1 has been reported in this cell type in kidney of rabbit [3, 7], rat [2, 4, 6], mouse [15, 16], chicken [17], and human [18], and in the homologous cell type in turtle bladder [19]. The major AE1 gene product expressed in mammalian type A IC is that encoded by the kAE1 mRNA [18, 20–22].

The kidney's ability to adapt to systemic acid/base perturbations has led several groups to investigate how modulation of AE1 expression might contribute to this adaptation. A two- to three-fold elevation of kAE1 mRNA levels was noted in both cortex and medulla of kidneys from rats maintained for five days in a 10% CO_2 atmosphere to produce chronic respiratory acidosis [23]. In contrast, rats subjected to metabolic acidosis or metabolic alkalosis for periods of 1 to 14 days showed no change in cortical or medullary levels of H^+-ATPase protein or mRNA. However, in these chronic studies the H^+-ATPase immunostaining pattern in IC demonstrated acidosis-induced shifts from intracellular vesicles to the cell surface, and alkalosis-induced shifts from the cell surface to intracellular vesicles [24].

In contrast, in a rat model of impaired urinary acidification induced by 24 hours ureteral obstruction, no change in IC H^+-ATPase localization was found for up to 10 days following obstruction. Although IC H^+-ATPase immunostaining intensity was elevated three hours following release of obstruction, it then returned to normal levels; AE1 was not analyzed [25]. Though no change in the AE1 immunostaining pattern was detected in rat kidney during hyperacute chloride depletion metabolic alkalosis [26], chronically increased distal chloride delivery achieved by six days of combined administration of bumetanide and NaCl led to decreased AE1 immunostaining in Type A IC, which were also noted to be reduced in size [27]. Chronic metabolic acidosis or alkalosis in late pregnancy and initial lactation of rats led to no changes in percent of Type A IC in the pups as defined by apical studs [28], an ultrastructural marker of the vacuolar H^+-ATPase [29]. However, the percent of Type B IC as defined by basolateral studs increased with maternal metabolic alkalosis and decreased with maternal metabolic acidosis [28].

In rabbit IC, AE1 immunostaining is found in intracellular vesicles and multivesicular bodies to a greater degree than in rat [30]. Chronic metabolic acidosis in the rabbit led to enhanced AE1 immunostaining at the IC surface and a reduced amount in intracellular vesicles [31]. Dissociated cortical collecting duct

Received for publication April 22, 1996
and in revised form July 31, 1996
Accepted for publication August 5, 1996

(CCD) cells prepared from rabbits subjected to subacute metabolic acidosis expressed four- to fivefold greater levels of AE1 RT-PCR product than did cells from rabbits with subacute metabolic alkalosis [14]. Acidosis may also have increased the level of kidney AE1 polypeptide in CCD cell lysates [14].

In the present study we have examined the effects of six hours metabolic (NH_4Cl) acidosis and metabolic ($NaHCO_3$) alkalosis on the expression in rat kidney of AE1 and of vacuolar H^+-ATPase, using indirect immunofluorescence to detect these transporter polypeptides. We focused on cortical IC in the late distal tubule, connecting segments, and the collecting duct, in view of the ability of the rat CCD rapidly to convert between net reabsorption and secretion of bicarbonate [32]. The results demonstrate that both perturbations acutely regulate the level of AE1 expression and the localization of H^+-ATPase in intercalated cells.

Methods

Animals

Adult male Sprague-Dawley rats were maintained on a standard diet and had free access to water. Metabolic acidosis was induced in the morning by gavage of 10 ml fluid containing (for acid loading) 3.5 mmoles ammonium chloride per 100 g body wt or (for alkali loading) 5.0 mmoles sodium bicarbonate per 100 g body wt. Control animals were gavaged with 10 ml of 140 mM sodium chloride. The animals were then allowed free access to tap water. Six hours following gavage, the animals were anesthetized with Nembutal (65 mg/kg, i.p.). Urine was withdrawn from the bladder into gas-tight syringes. The abdominal aorta was cannulated, and arterial blood was withdrawn into heparinized, gas-tight syringes. The animals then underwent retrograde perfusion via the aorta with Hank's balanced solution until the kidneys were thoroughly blanched, and then perfusion-fixed with 2% paraformaldehyde/75 mM lysine/10 mM sodium periodate (PLP) as previously described [6, 33]. Kidneys were excised, cut into blocks of cortex, medullary outer stripe and inner stripe, and further fixed in PLP overnight at 4°C. Fixed tissue blocks were washed four times with PBS, then stored at 4°C in PBS containing 0.02% sodium azide until further use.

Antibodies

The murine monoclonal antibody to the 31 kDa subunit of bovine inner medullary vacuolar H^+-ATPase has been verified previously to cross-react with the rat kidney protein [5, 6, 33]. The affinity-purified rabbit polyclonal antibody to the carboxy-terminal 12 amino acids 1224-1237 of mouse AE2 [34] cross-reacts with rat AE1, and recognizes in semithin sections of kidney only AE1 and not AE2 when used as an immunostaining reagent with the described fixation and incubation conditions [15, 35]. AE1 immunostaining patterns were verified with specific anti-AE1 antipeptide antibodies [6]. Fluorescein-conjugated goat anti-mouse IgG and Texas Red-conjugated goat anti-rabbit IgG were obtained from Jackson Immunochemicals.

Immunocytochemistry

Fixed tissue blocks were successively infiltrated with 1.6 M or 2.3 M sucrose in PBS/azide, frozen in liquid nitrogen, and sectioned at 4 to 5 μm thickness on a Reichert Frigocut cryostat, or at 1 μm thickness on a Reichert Ultracut E cryostat. Sections were placed on Superfrost/Plus Microscope Slides (Fisher) and stored in PBS/azide at 4°C until use, or alternatively stored at −20°C for longer periods.

Indirect immunofluorescence detection was performed as previously described [6, 15]. Sections were preincubated at room temperature in PBS for 10 minutes, in 1% bovine serum albumin (BSA) in PBS for 15 minutes, then incubated at room temperature for one to two hours with either primary antibody as indicated or with pooled nonimmune serum. Many sections were subjected to a double-incubation procedure. Sections were washed twice for five minutes in PBS containing added 2.7% NaCl (high-salt PBS) and twice in normal PBS. The sections were then incubated for one hour with fluorophore-conjugated secondary antibodies (at concentrations of 10 to 15 μg/ml), followed by two washes of five minutes each in high-salt PBS and two washes in normal PBS. Sections were mounted in 50% glycerol in 0.2 M Tris-HCl, pH 8.0, containing 2.5% n-propylgallate as an antiquenching agent.

Sections were examined and photographed with a Nikon FXA photomicroscope equipped for epifluorescence and photographed using Kodak TMAX 400 film push-processed to 1600 ASA. Distal tubules, connecting segments, and collecting ducts were identified on the basis of morphological criteria that have been previously described. The number, shape, and size of IC as well as of surrounding cells is characteristic for each of these segments. In addition, H^+-ATPase clearly stains the apical plasma membrane but very few cytoplasmic vesicles of all cells in the distal tubule, as well as many non-IC in the connecting segment. In contrast, principal cells (PC) in the CCD show much less apical staining. Immunocytological categories of IC were assigned according to a modification of the categories described previously for the rabbit [7] and the rat [24, 36]. Only cells in which the nucleus was identified were counted in quantitative analyses in order to minimize histologic misreading secondary to tangential sections. On average, 200 to 250 cortical IC were examined in each of five control and alkalotic rats, and in each of four acidotic rats. IC were categorized for AE1 immunostaining intensity and for distribution pattern of H^+ ATPase. Statistical significance of the differences between control and acidotic values, between control and alkalotic values, and between acidotic and alkalotic values for given measurements were assessed by Student's two-tailed t-test for two samples assuming equal variances. $P < 0.05$ was considered statistically significant.

Some sections were examined and image files acquired with a BioRad MRC600 laser confocal scanning microscope. For quantitative confocal analysis of AE1 staining intensity, 5 μm sections stained by indirect immunofluorescence were used. Sections used for quantitation were cut from control, acidotic, and alkalotic tissue and stained at the same time with the same preparations of diluted primary and secondary antibodies. Sections from control rats were mounted on the confocal microscope stage, and tubule segments containing stained cells were identified. The section was rapidly scanned to find the point along the stained membrane where the fluorescence was subjectively the brightest, and parameters for aperture size, gain, and black level were optimized for the control tissue, so that the brightest pixel intensities were readily visible without further image enhancement, but remained well below saturation (255 grey-scale units). These values held constant for quantification for subsequent control and experimental tissue samples. Up to ten stained tubules per region of section

Table 1. Acid/base parameters

	Control (N = 12)	Acidosis (N = 15)	Alkalosis (N = 13)
Blood pH	7.34 ± 0.01	6.97 ± 0.02[a]	7.48 ± 0.01[a]
pCO_2 *mm Hg*	42.3 ± 1.9	40.0 ± 2.4	47.6 ± 1.3[c]
pO_2 *mm Hg*	87.8 ± 3.3	97.0 ± 6.9	86.5 ± 3.3
$[HCO_3^-]$ *mM*	22.9 ± 0.7	9.2 ± 0.5[a]	35.3 ± 0.7[a]
Urine pH	6.8 ± 0.2	5.5 ± 0.1[b]	8.4 ± 0.1[b]

Parameters at time of sacrifice, 6 hrs after gavage administration of acid or base. Values are means ± SEM. N = number of rats. Urine pH values were from 6 controls, 8 acid-treated, and 6 alkali-treated animals.

[a] $P < 0.00001$; [b] $P < 0.002$; [c] $P < 0.05$, each compared to corresponding control value

were scanned and saved using the Kalman frame-averaging algorithm supplied with the BioRad software. The images were saved on a 44 Mb SyQuest removable hard disk.

For quantification of labeling, images were retrieved and the magnification was digitally increased to facilitate analysis. The area of basolateral fluorescence staining on each cell was outlined with the area tracer tool supplied with the softward package, and the mean pixel intensity of the enclosed area was recorded. The area outlined was not the same for each cell, but this method provided data that were independent of stained surface area. For each experimental condition, immunostaining intensities from one section from each of four or five rats were quantitated. Mean pixel intensities were loaded into the Statworks program, and means ± sem were calculated, together with P values using Student's two-tailed t-test for paired and unpaired samples.

Results

Systemic acid/base parameters

The acid/base state of the rats at time of sacrifice, 6 ± 0.5 hours post-gavage, is summarized in Table 1. Ammonium chloride gavage produced acute metabolic acidosis, with blood pH 6.97, serum bicarbonate 9.2 mM, and urine pH 5.5, compared to control values of 7.34, 22.9 mM, and 6.8, respectively. However, the acidotic animals did not mount a significant compensatory respiratory alkalosis that was evident at time of sacrifice. Thus, the "NH_4Cl acidosis" was a combined metabolic-respiratory acidosis.

Sodium bicarbonate gavage produced acute metabolic alkalosis, with blood pH 7.48, serum bicarbonate 35.3 mM, and urine pH 8.4. Slight compensatory respiratory acidosis was already evident in the alkalotic animals, with pCO_2 of 47.6 mm Hg compared to the control value of 42.3 mm Hg ($P < 0.05$). The animals remained in otherwise satisfactory condition, as evidenced by unchanged arterial pO_2 values.

Immunocytochemical changes in IC from acidotic and alkalotic animals

IC were defined as cells which displayed immunostaining for either H^+ ATPase, AE1, or both proteins. As shown in Figure 1, IC were easily identified in cortical collecting ducts (CCD) in all conditions. As noted previously, H^+-ATPase was found on either surface or both surfaces of CCD IC. In contrast, AE1 was observed uniquely on basolateral membranes of a subset of IC, as we and others have previously noted. No AE1 was detected in apical membranes within any renal tubule segment with the antibody presented or with four other anti-AE1 antibodies which immunostain red blood cells (not shown).

Though approximately equal numbers of AE1-positive and AE1-negative cells were present in connecting segments (CNT) and in CCD (Table 2), some CCD in semithin sections exhibited predominantly one IC type or the other, as reported previously in isolated perfused rabbit CCD for functionally defined IC [37]. Therefore, in the double-stained section of control kidney shown in Figure 1, most of the IC present in the CCD are of morphological Type A (closed arrow), with apical H^+-ATPase and basolateral AE1. Also present are morphological Type B cells (arrowhead), characterized by basolateral and/or diffuse localization of H^+ ATPase and no detectable AE1 immunostaining. In addition, the CCD shown contains one IC that exhibits uniquely or predominantly apical H^+ ATPase in the absence of AE1 immunostaining (asterisk). Such sections were previously reported, and termed "novel" IC [6]. As reported earlier [6, 33], the proximal tubule brush border microvillar crypts also exhibit H^+-ATPase staining without AE1 staining.

In kidneys from acidotic animals (Fig. 2), H^+-ATPase staining was enhanced by concentration at the apical surface of Type A cells (Fig. 2A, arrow), while Type B cells (arrowhead) retained or enhanced the basolateral concentration of H^+-ATPase staining. In Type A cells from acidotic animals, basolateral AE1 staining was also intensified (Fig. 2B, arrow) compared to control CCD, whereas Type B cells remained AE1-negative (Fig. 2B, arrowhead). Total H^+-ATPase staining in IC of Type A or Type B showed no consistent changes in acute acidosis or alkalosis.

In kidneys from alkalotic animals (Fig. 3), IC with H^+-ATPase staining at the basolateral cell surface of Type B cells were more numerous (Fig. 3A, arrowhead), and the basolateral staining intensity also appeared increased. AE1 immunostaining in Type A cells was decreased in intensity, and was sometimes dramatically reduced (Fig. 3B, arrow).

Effects of acute acidosis and alkalosis on AE1 status of IC

The effects of acute acidosis and alkalosis on the relative numbers of IC subtypes were quantitated separately in the CNT (including the late distal tubule) and in the CCD. IC comprised 45% of total cells in the connecting segment. The % of CNT IC which were $AE1^+$ was 54.2% in control animals, 57.6% in acidotic animals, and 54.4% in alkalotic animals (Table 2). These proportions in acidotic and alkalotic animals were not different from control or from each other ($P > 0.5$). In the CCD, IC comprised 59% of total cells, a number that is higher than reported in previous rat studies which combined CNT and CCD. The % of CCD IC which were $AE1^+$ was 53.7% in control animals, 56.4% in acidotic animals, and 43.9% in alkalotic animals (Table 2). In the CCD, acid-base status produced a tendency to change the % of IC which expressed detectable AE1, but these shifts did not reach statistical significance ($P > 0.2$ for either experimental group compared to control, $P > 0.07$ for acidotic compared with alkalotic). AE1 expression status is one light microscopic criterion by which Type A and Type B cells are defined. Another major criterion is localization of H^+-ATPase [5]. By this criterion, as well, relative proportions of Type A and Type B cells were not significantly changed by NH_4Cl acidosis or by $NaHCO_3$ alkalosis ($P > 0.1$).

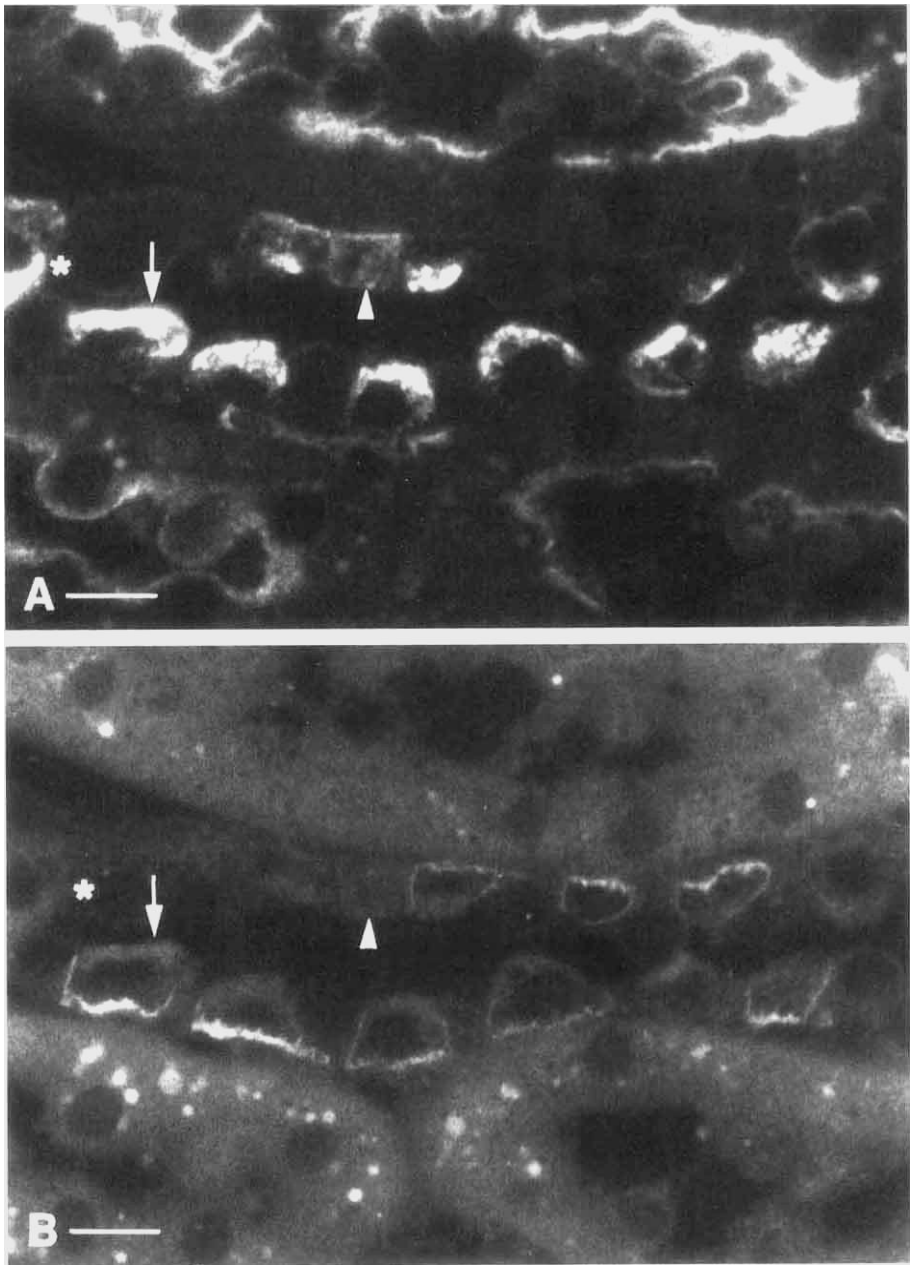

Fig. 1. *Semithin cryosection (1 μm thickness) of rat CCD taken from a control animal.* Section was double-immunostained with monoclonal antibody to H^+-ATPase (**A**) and with polyclonal antibody to AE1 (**B**). Closed arrow indicates IC of morphologic Type A; arrowhead indicates IC of morphologic Type B. Asterisk (at left of panels) indicates IC with apical H^+-ATPase and undetectable AE1. Proximal tubules above and below the centrally situated horizontal CCD display H^+-ATPase staining at base of apical brush border (A) without AE1 staining (B). Proximal tubules in both panels display lysosomal autofluorescence. Bar represents 10 μm.

Effects of acute acidosis and alkalosis on AE1 immunostaining intensity

The intensity of AE1 immunostaining in $AE1^+$ IC was semiquantitatively assessed by laser confocal scanning fluorescence microscopy (Table 3). The entire basolateral pole of each measured IC was included in the measurement. AE1 pixel intensity in acidotic animals increased by 12% compared to control values, whereas AE1 pixel intensity in alkalotic animals decreased by 27% compared to control values (for both perturbations, $P > 0.001$ compared to control). Background pixel intensity averaged 40 ± 7 gray scale units in control cells and 28 ± 7 units in alkalotic cells. With these background correction values, the average decrease in AE1 immunostaining intensity in the basolateral membrane of cortical A-type IC of alkalotic animals remained 26%. Similar measurements in the outer medullary inner stripe revealed a 12% increase in pixel intensity in IC from acidotic rats, but no significant intensity change in IC from alkalotic rats (data not shown).

Table 2. Effects of acid/base perturbation on AE1 status of cortical IC

	Control (5)	Acidosis (4)	Alkalosis (5)
Connecting segment			
$AE1^+$ *% of IC*	54.2 ± 5.8	57.6 ± 5.9	54.4 ± 2.4
$AE1^-$ *% of IC*	45.8 ± 5.8	42.4 ± 5.9	45.6 ± 2.4
Cortical collecting duct			
$AE1^+$ *% of IC*	48.0 ± 1.8	52.7 ± 2.9	43.1 ± 3.1
$AE1^-$ *% of IC*	52.0 ± 1.8	47.3 ± 2.9	56.9 ± 3.1

Values are means ± SEM from 4 or 5 animals, with >400 total cells counted per animal. Acidotic and alkalotic values did not differ from control values ($P > 0.2$).

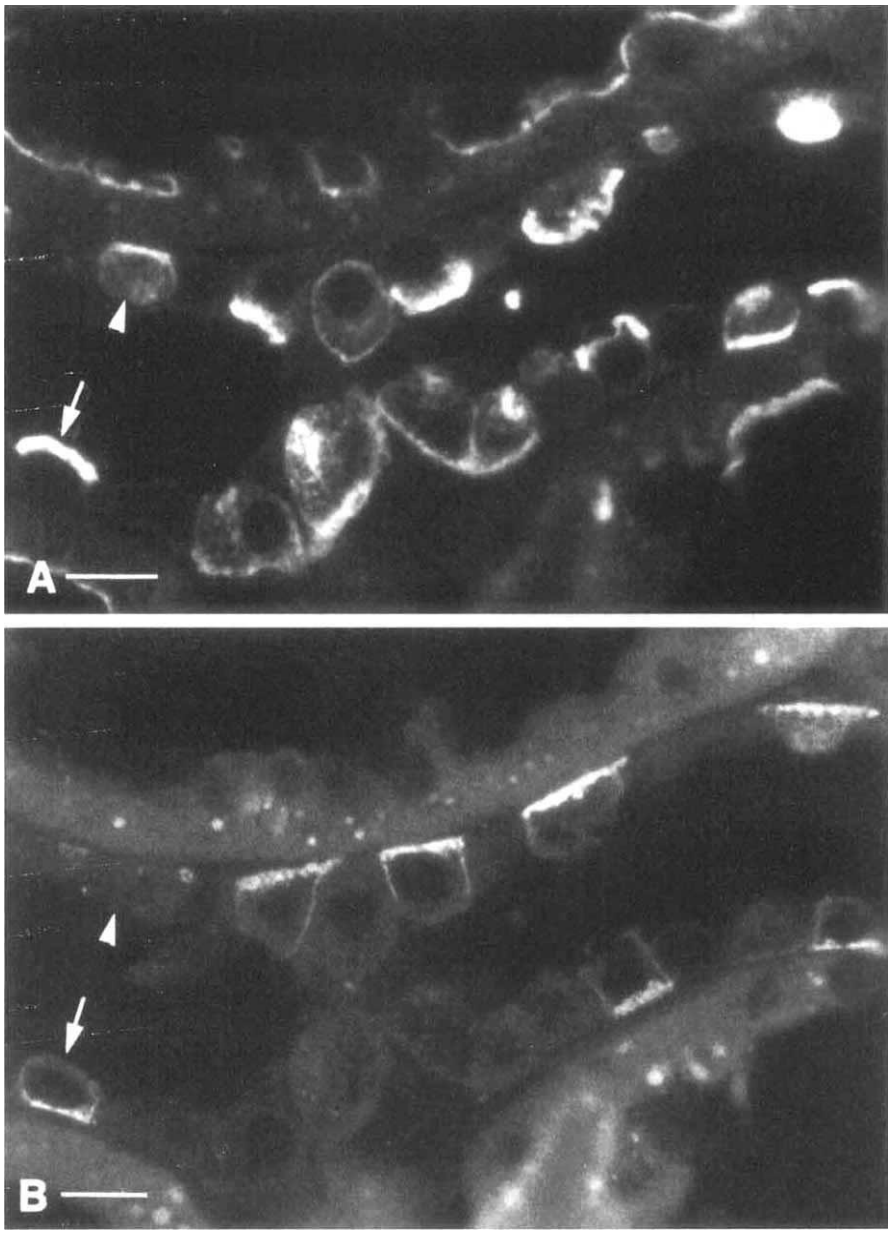

Fig. 2. *Semithin (1 μm) cryosection of rat CCD taken from an animal with acute metabolic acidosis, double-immunostained with monoclonal antibody to H^+-ATPase* (**A**) *and with polyclonal antibody to AE1* (**B**). Basolateral AE1 staining of type A IC (arrow in B) is enhanced, and apical H^+-ATPase staining of type A IC is more linear and less diffuse than in control rats. Symbols as in Figure 1. Bar represents 10 μm.

Effects of acute acidosis and alkalosis on IC cell subtypes as defined by H^+-ATPase distribution

A spectrum of IC types has been described in the rat CCD based on the distribution of vacuolar H^+-ATPase immunostaining in chronic metabolic acidosis [14]. Therefore, the effects of acute acidosis and alkalosis on AE1 immunostaining intensity and distribution were evaluated as a function of H^+-ATPase distribution within IC (summarized in Fig. 4). Table 4 shows the matrix of IC types present in the control rat connecting segment, whereas Tables 5 and 6 present the cell type distribution present in acidotic and alkalotic animals, respectively. NH_4Cl acidosis increased the proportion of strong and medium $AE1^+$ cells with apical or apical/diffuse H^+-ATPase. Acidosis may have correspondingly decreased the proportion of weak $AE1^+$ cells with apical/diffuse H^+-ATPase (Table 5). $NaHCO_3$ alkalosis shifted every cell phenotype of H^+-ATPase towards weaker AE1 immunostaining, but only minimally shifted the H^+-ATPase phenotype among $AE1^-$ IC from apical towards basolateral distribution (Table 6).

Figure 4 summarizes in bar graph form the data from Tables 4 to 6. In connecting segment of control animals, most IC exhibited apical/diffuse H^+-ATPase, and a range of AE1 staining intensities. Acidosis shifted the pattern of cell types towards stronger AE1 staining intensity and tighter apical localization of H^+-ATPase. Alkalosis shifted the pattern towards weaker AE1 staining intensity, but redistribution of H^+-ATPase was minimal.

Table 7 shows the matrix of IC types present in the control rat CCD, whereas Tables 8 and 9 present the CCD cell types in acidotic and alkalotic animals, respectively. NH_4Cl acidosis significantly increased the proportion of strong $AE1^+$ cells which displayed apical or apical/diffuse H^+-ATPase, with corresponding

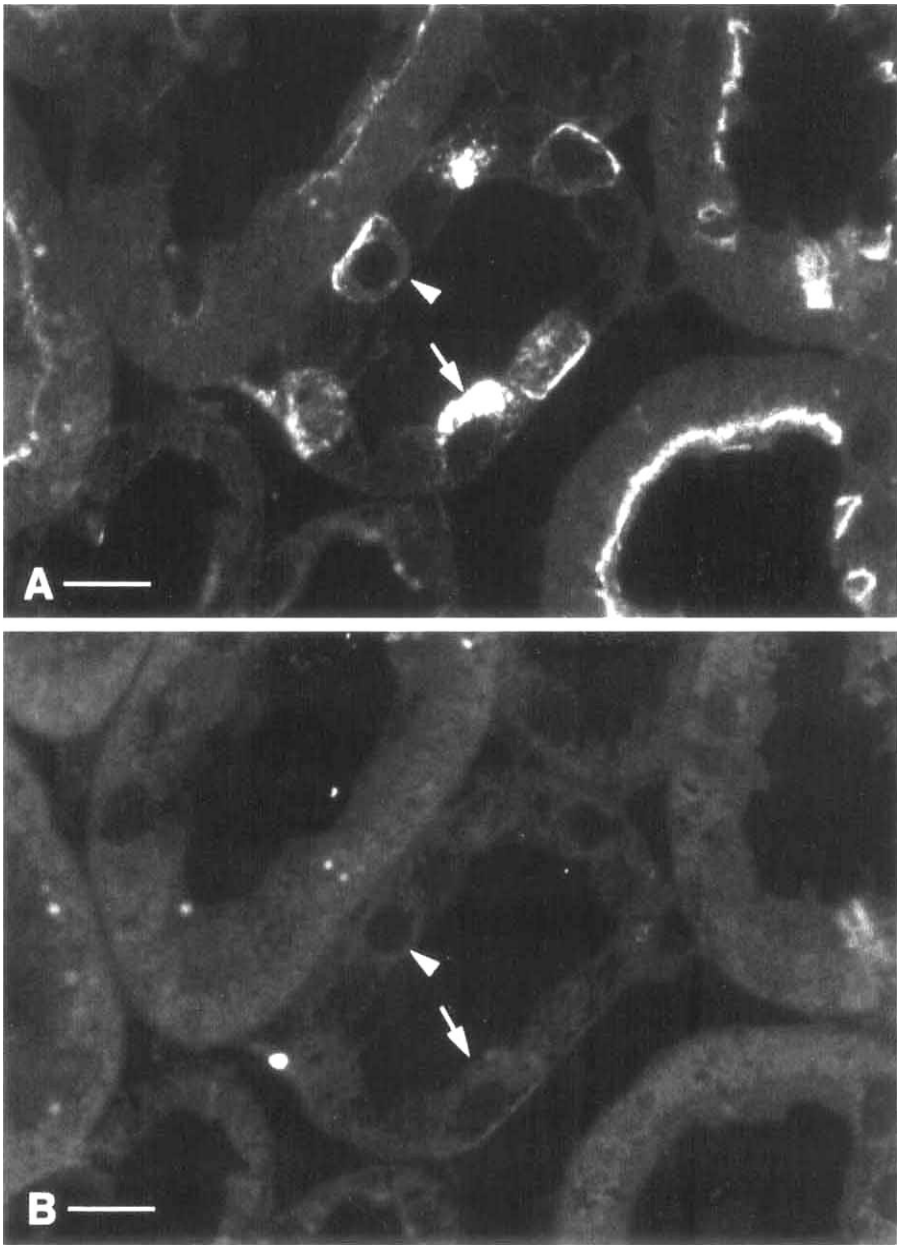

Fig. 3. *Semithin (1 μm) cryosections of rat CCD taken from an animal with acute metabolic alkalosis, double-immunostained with monoclonal antibody to H^+-ATPase* (**A**) *and with polyclonal antibody to AE1* (**B**). Basolateral H^+-ATPase staining of type B IC is increased (arrowhead in A), whereas basolateral AE1 staining of type A IC is often dramatically reduced (arrow in B). Symbols as in Figure 1. Bar represents 10 μm.

Table 3. Confocal immunostaining intensity of rat cortex AE1

Group	Pixel intensity *mean + SEM (N)*	*P*
Control	102.9 ± 2.1 (57)	—
Acidotic	115.4 ± 2.6 (51)	< 0.001
Alkalotic	74.7 ± 2.5 (49)	< 0.0001

Pixel intensities of basolateral surfaces of AE1-positive cortical IC were measured in 0.5 μm optical sections (see **Methods**).

reductions in medium and weak $AE1^+$ cells, especially among apical/diffuse H^+-ATPase cells. $NaHCO_3$ alkalosis produced a moderate decrease in the proportion of strong $AE1^+$ cells, which displayed apical or apical/diffuse H^+-ATPase compared to controls. However, to a greater degree than in the connecting segment, alkalosis shifted H^+-ATPase from apical localization towards diffuse and basolateral localizations among $AE1^-$ cells.

Figure 5 similarly summarizes in bar graph form the data from Tables 7 to 9. The major changes induced by acidosis and alkalosis in CCD paralleled those observed in connecting segment. Hence, acidosis shifted the IC distribution towards strong AE1 staining intensity and a more apical distribution of H^+-ATPase. Alkalosis decreased AE1 staining intensity, and shifted H^+-ATPase away from the apical surface. Figures 4 and 5 also emphasize a difference between IC of the connecting segment and the CCD. The connecting segment had very few $AE1^-$ IC which showed basolateral or basolateral/diffuse H^+-ATPase distribution, even in alkalosis. In contrast, the CCD showed substantial numbers of these cells, which increased in proportion in the alkalotic state.

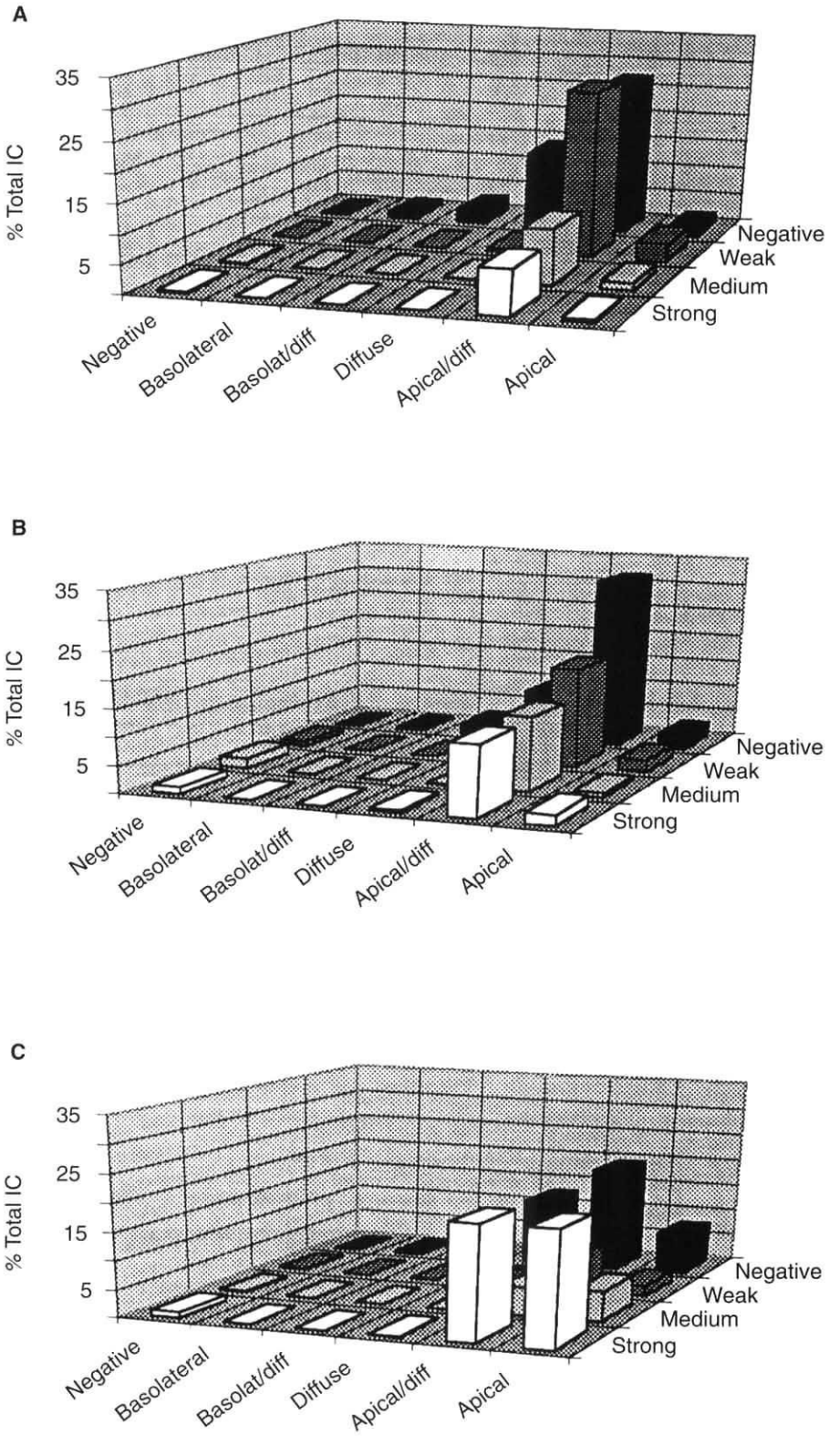

Fig. 4. *Summary of immunostaining profiles of IC in CNT in alkalotic (***A***), control (***B***), and acidotic conditions (***C***).* The % of total IC is plotted on the *z* axes, AE1 immunostaining intensity is plotted on the *y* axes (from foreground to background in the order: strong, medium, weak, and AE1-negative). Immunolocalization pattern of H^+-ATPase is plotted on the *x* axes (from left to right in the order: negative, basolateral, basolateral/diffuse, diffuse, apical/diffuse, and apical). Data taken from Tables 4 to 6.

Well-polarized basolateral H^+-ATPase was found only in $AE1^-$ IC. These comprised 3.9 ± 1.6% of IC in control CCD, and increased to 11.1 ± 3.1% of IC in alkalotic rats ($P < 0.05$). In acidotic rats the proportion of this cell type showed no significant change in CCD compared to controls.

IC which displayed basolateral and basolateral/diffuse staining

Table 4. AE1 phenotypes of IC in the control CNT

AE1 immunostaining intensity	vH^+-ATPase immunostaining phenotype % ± SEM of total intercalated cells						
	Apical	Apical/ diffuse	Diffuse	Basolat/ diffuse	Basolat	Negative	Total
Strong (+++)	1.9 ± 0.7	12.8 ± 4.4	0.4 ± 0.2	0	0	1.3 ± 0.6	16.4
Medium (++)	0.9 ± 0.3	13.4 ± 4.0	0.04 ± 0.04	0	0	1.9 ± 1.0	16.2
Weak (+)	2.2 ± 0.9	18.3 ± 4.2	0.2 ± 0.2	0	0	0.9 ± 0.2	21.6
Negative (−)	2.7 ± 0.7	31.5 ± 6.8	9.5 ± 3.7	1.9 ± 0.8	0.4 ± 0.2	n.a.	46.0
Total	7.7	76.0	10.1	1.9	0.4	4.1	

Values are from 1228 intercalated cells in 5 animals (246 ± 59 intercalated cells per animal). Intercalated cells were defined by the presence of immunostaining with antibodies to either or both AE1 or vH^+-ATPase. Abbreviation n.a. is not applicable.

Table 5. AE1 phenotypes of IC in the acidotic CNT

AE1 immunostaining intensity	vH^+-ATPase immunostaining phenotype % ± SEM of total intercalated cells						
	Apical	Apical/ diffuse	Diffuse	Basolat/diffuse	Basolat	Negative	Total
Strong (+++)	20.2 ± 5.5[a]	20.2 ± 2.4[c]	0.1 ± 0.1	0	0	1.1 ± 1.1	41.6
Medium (++)	5.3 ± 2.0[b]	5.0 ± 1.6	0	0	0	0.2 ± 0.2	10.5
Weak (+)	1.9 ± 1.0	6.3 ± 2.2[b]	0.2 ± 0.2	0	0	0.2 ± 0.2[b]	8.6
Negative (−)	7.6 ± 1.1[a]	19.2 ± 2.9	12.4 ± 2.5	2.9 ± 0.9	0.4 ± 0.2	n.a.	42.5
Total	35.0	50.7	12.7	2.9	0.4	1.5	

Values are from 822 intercalated cells in 4 animals (206 ± 56 intercalated cells per animal). Intercalated cells were defined by the presence of immunostaining with antibodies to either or both AE1 or vH^+-ATPase. Abbreviation n.a. is not applicable.

[a] $P \leq 0.01$ vs. the same cell type in control animals

[b] $P \leq 0.05$ vs. the same cell type in control animals

[c] $P < 0.005$ vs. the same cell type in alkalotic but not control animals

Table 6. AE1 phenotypes of IC in the alkalotic CNT

AE1 immunostaining intensity	vH^+-ATPase immunostaining phenotype % ± SEM of total intercalated cells						
	Apical	Apical/ diffuse	Diffuse	Basolat/ diffuse	Basolat	Negative	Total
Strong (+++)	0.5 ± 0.3[a]	7.8 ± 1.7[a]	0	0	0	0.3 ± 0.1	8.6
Medium (++)	1.3 ± 0.3[b]	9.7 ± 1.7[a]	0.1 ± 0.3	0	0	0.1 ± 0.1	11.2
Weak (+)	3.3 ± 1.4	29.0 ± 2.6[a]	0.5 ± 0.4	0	0	1.2 ± 0.2[b]	34.0
Negative (−)	1.6 ± 0.6	27.0 ± 1.3	13.8 ± 1.2	2.4 ± 0.4	1.0 ± 0.3	n.a.	45.8
Total	6.7	73.5	14.6	2.4	1.0	1.6	

Values are from 1133 intercalated cells in 5 animals (227 ± 19 intercalated cells per animal). Intercalated cells were defined by the presence of immunostaining with antibodies to either or both AE1 or vH^+-ATPase. Abbreviation n.a. is not applicable.

[a] $P < 0.005$ vs. acidotic but not control animals

[b] $P < 0.05$ vs. acidotic but not control animals

for H^+-ATPase were uniformly AE1-negative. AE1-expressing IC which displayed diffuse staining for H^+-ATPase represented fewer than 1.0% of total IC, and usually less than 0.5%. These three groups of IC fit the profile of Type B IC both as characterized by H^+-ATPase staining (basolateral, basolateral/diffuse, and diffuse) and by absence of detectable basolateral AE1. This category of AE1-negative cells with concentration of H^+-ATPase at or towards the basal pole of the cell, as well as that with diffuse H^+-ATPase localization, was more numerous in CCD than in CNT regardless of acid-base status. Conversely, $AE1^-$ cells which in acidosis displayed apical or apical/diffuse distributions of H^+-ATPase were more numerous in CNT than in CCD, again regardless of acid-base status (Fig. 2).

The "basolateral/diffuse" category of cells in Tables 4 to 9 includes IC with well-polarized, bipolar localization of H^+-ATPase, as originally described by Brown, Hirsch and Gluck [33]. These bipolar cells comprised 1.7 ± 0.7% of connecting segment IC, and 3.4 ± 1.3% of CCD IC. Alkalosis produced only a suggestive reduction of these respective values to 0.3 ± 0.1% and 1.0 ± 0.3% ($P = 0.1$), in contrast to the increases reported previously [24].

The proportions of IC which were AE1-negative but apical H^+-ATPase-positive increased in abundance in the CNT of acidotic rats from the control value of 2.7 ± 0.7% to 7.6 ± 1.1% ($P < 0.05$). This type of IC showed no change in the CCD. A cell type not previously reported was also detected in both CNT and CCD. This basolateral AE1-positive, H^+-ATPase-negative cell type represented 4.1% and 4.3% of IC in the control CNT and CCD, respectively. In CCD, acidosis increased and alkalosis decreased AE1 staining intensity in this cell type. In addition, alkalosis decreased the proportion of cells of this type detected in CCD from 3.4 ± 1.3 to 1.0 ± 0.3% ($P < 0.05$). In CNT both

Table 7. AE1 phenotypes of IC in the control CCD

AE1 immunostaining intensity	vH^+-ATPase immunostaining phenotype % ± *SEM of total intercalated cells*						
	Apical	Apical/ diffuse	Diffuse	Basolat/ diffuse	Basolat	Negative	Total
Strong (+++)	1.9 ± 0.5	8.5 ± 2.6	0	0	0	0.8 ± 0.02	11.2
Medium (++)	1.9 ± 0.3	10.3 ± 1.3	0.1 ± 0.1	0	0	2.0 ± 0.7	14.3
Weak (+)	2.0 ± 0.7	18.8 ± 3.7	0.1 ± 0.1	0	0	1.5 ± 0.6	22.4
Negative (−)	1.9 ± 0.8	16.2 ± 4.8	20.1 ± 4.6	9.9 ± 2.7	3.9 ± 1.6	n.a.	52.0
Total	7.7	53.8	20.3	9.9	3.9	4.3	

Values are from 1065 intercalated cells in 5 animals (213 ± 40 intercalated cells per animal). Intercalated cells were defined by the presence of immunostaining with antibodies to either or both AE1 or vH^+-ATPase. The category "basolateral/diffuse" in this and subsequent tables includes "bipolar cells" with condensed vH^+-ATPase immunostaining on both basolateral and apical membranes as previously described in ref. 24. Abbreviation n.a. is not applicable.

Table 8. AE1 phenotypes of IC in the acidotic CCD

AE1 immunostaining intensity	vH^+-ATPase immunostaining phenotype % ± *SEM of total intercalated cells*						
	Apical	Apical/ diffuse	Diffuse	Basolat/ diffuse	Basolat	Negative	Total
Strong (+++)	15.0 ± 2.4[a]	23.6 ± 3.7[a]	0.4 ± 0.3	0	0	2.1 ± 0.7[b]	41.1
Medium (++)	2.4 ± 0.8	4.6 ± 0.7[a]	0	0	0	0.5 ± 0.2	7.5
Weak (+)	0.5 ± 0.5[b]	3.3 ± 2.1[a]	0.2 ± 0.2	0	0	0.2 ± 0.2	4.2
Negative (−)	2.3 ± 1.2	8.9 ± 0.9	21.4 ± 3.6	9.2 ± 2.7	5.4 ± 2.1	n.a.	47.2
Total	20.2	40.4	22.0	9.2	5.4	2.8	

Values are from 893 intercalated cells in 4 animals (223 ± 22 intercalated cells per animal). Intercalated cells were defined by the presence of immunostaining with antibodies to either or both AE1 or vH^+-ATPase. Abbreviation n.a. is not applicable.

[a] $P < 0.05$ vs. control animals

[b] $P < 0.05$ vs. alkalotic but not control animals

Table 9. AE1 phenotypes of IC in the alkalotic CCD

AE1 immunostaining intensity	vH^+-ATPase immunostaining phenotype % ± *SEM of total intercalated cells*						
	Apical	Apical/ diffuse	Diffuse	Basolat/ diffuse	Basolat	Negative	Total
Strong (+++)	0.4 ± 0.1[a]	5.0 ± 0.9[c]	0.2 ± 0.2	0	0	0.3 ± 0.1[a]	5.0
Medium (++)	0.8 ± 0.4[a]	8.1 ± 1.6	0.1 ± 0.1	0	0	0.5 ± 0.2	9.5
Weak (+)	3.3 ± 0.5[b]	23.5 ± 2.8[c]	0.7 ± 0.3	0	0	0.3 ± 0.2	27.8
Negative (−)	1.1 ± 0.3	9.3 ± 2.0	21.9 ± 4.5	13.5 ± 1.3	11.1 ± 3.1[a]	n.a.	56.9
Total	5.6	45.9	22.9	13.5	11.1	1.1	

Values are from 1254 intercalated cells in 5 animals (251 ± 49 intercalated cells per animal). Intercalated cells were defined by the presence of immunostaining with antibodies to either or both AE1 or vH^+-ATPase. Abbreviation n.a. is not applicable.

[a] $P < 0.05$ vs. control animals

[b] $P < 0.02$ vs. acidotic but not control animals

[c] $P < 0.001$ vs. acidotic but not control animals

acidosis and alkalosis decreased the AE1 staining intensity of this cell type. It remains possible that this cell type, categorized here as a distinct, observed entity, represents an artifact of sectioning at 4 to 5 μm thickness.

Discussion

The present study is the first to examine the coordinate modulation of immunohistochemically-detected anion exchanger AE1 and H^+-ATPase in IC of rat CNT and CCD in response to acute NH_4Cl acidosis and acute $NaHCO_3$ alkalosis. Rats were examined six hours after enteral administration of a single acid or base load sufficient to produce acute systemic acidosis and alkalosis, respectively. Vacuolar H^+-ATPase underwent redistribution within IC towards the apical cell pole during acute acidosis, as was reported previously for subacute and chronic acid/base perturbations. In acute alkalosis, significant redistribution of H^+-ATPase toward the basal cell pole was noted in $AE1^-$ cells of CCD and to a lesser extent in $AE1^-$ cells of CNT, but was undetected in $AE1^+$ IC of either segment. Localization of AE1, as detected in semithin sections of 1 and 5 μm thickness, remained restricted to the IC basolateral membrane in all experimental conditions. Expression levels of AE1 as determined by semiquantitative confocal microscopy decreased in acute alkalosis and increased less dramatically in acidosis in both CNT and in CCD. Whether IC were scored by AE1 expression or by H^+-ATPase localization, the observed changes in proportions of Type A and Type B IC in acidosis and in alkalosis did not achieve statistical significance. Thus, the current study does not provide support for the hypothesis that Type A and Type B IC undergo interconversion during

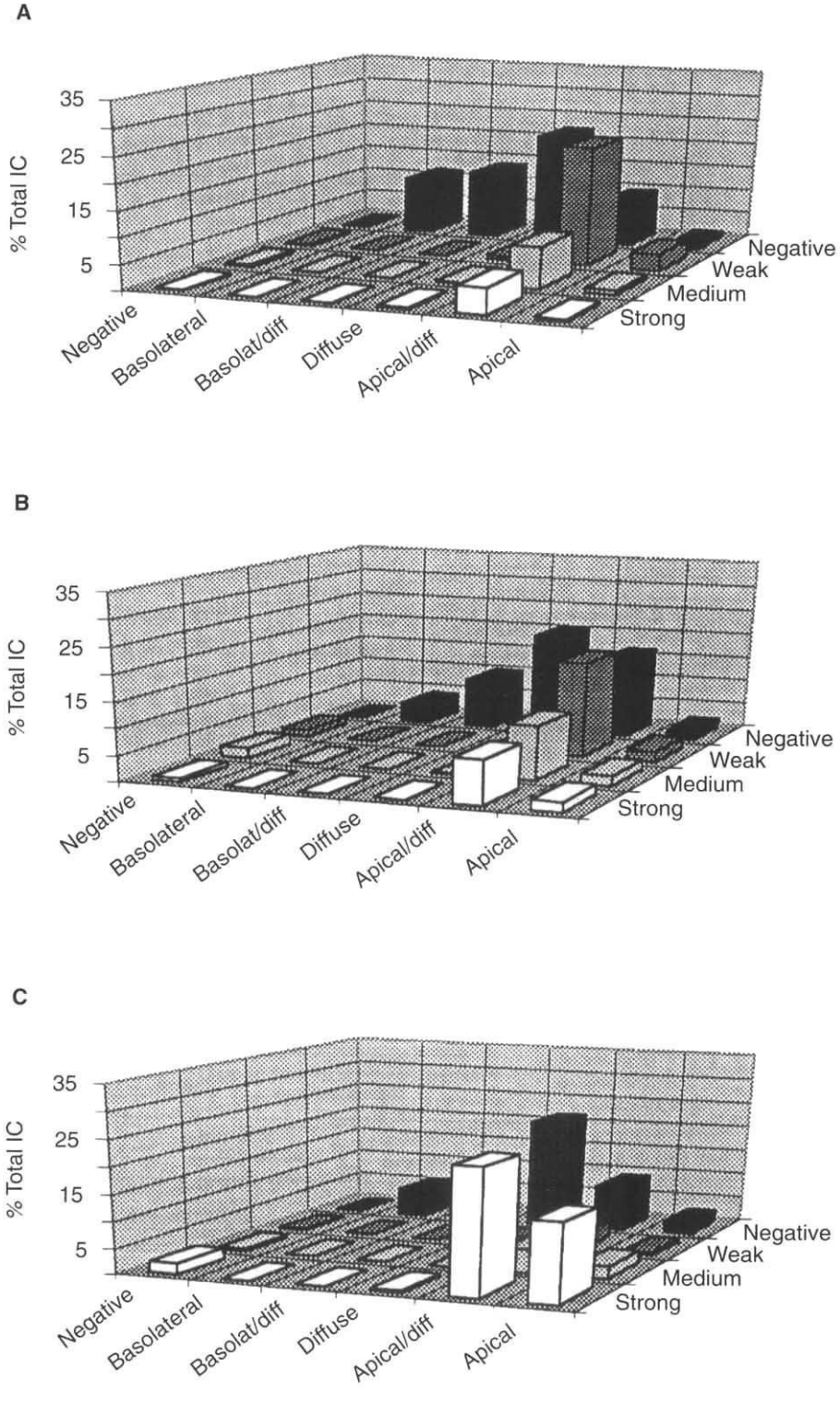

Fig. 5. *Summary of immunostaining profiles of IC in CCD in alkalotic* (**A**)*, control* (**B**)*, and acidotic conditions* (**C**). The % of total IC is plotted on the *z* axes, AE1 immunostaining intensity is plotted on the *y* axes (from foreground to background in the order: strong, medium, weak, and AE1-negative). Immunolocalization pattern of H^+-ATPase is plotted on the *x* axes (from left to right in the order: negative, basolateral, basolateral/diffuse, diffuse, apical/diffuse, and apical). Data taken from Tables 7 to 9.

adaptation to systemic acid/base perturbations [38]. (Neither, however, do the data disprove the hypothesis.)

One previous immunocytochemical study has examined hyperacute (2 hr) metabolic alkalosis in the rat [26]. This chloride-depletion metabolic alkalosis was induced by 30 minutes of peritoneal dialysis followed by 90 minutes of intravenous infusion of 80 mM chloride, at which time the animals were sacrificed for study. The systemic alkalosis was of equivalent magnitude to that in the present study, but likely of more rapid onset. The degree of respiratory compensation was also equivalent. The base load and elapsed time sufficed to convert subsequently isolated and perfused CCD segments from a state of net bicarbonate reabsorption

to sustained net bicarbonate secretion [32]. As previously reported in rabbit CCD, bicarbonate reabsorption in rat CCD required bath chloride, consistent with a requirement for a basolateral anion exchanger with a localization similar to that of AE1. These investigators later found in the same model of hyperacute alkalosis no change in the distribution of AE1 in basolateral membranes of Type A IC, as detected by immunogold labeling at the ultrastructural level [26].

In contrast to the present study, however, hyperacute metabolic alkalosis produced no reported change in AE1 level of expression [26]. The decreased expression of AE1 observed in the present study might be related to the different durations and possibly different rates of onset of alkalosis, as well as to possible differences in resolution between immunogold electron microscopy and immunofluorescence light microscopy using different antibodies.

After six days of treatment of rats with bumetanide and NaCl loading, CCD AE1 detected by immunoelectron microscopy was also decreased [27]. In this study, chronic diuresis led to the occasional detection of AE1 immunostaining in lysosome-like structures. In contrast to the rat, AE1 in the CCD of normal rabbits was found to be predominantly localized to intracellular structures of Type A IC, but twelve days of sustained metabolic acidosis led to decreased AE1 immunostaining inside cells and intensification of staining in the basolateral membranes [31]. This difference between rats and rabbits correlates with the greater dietary alkali load and a more alkaline urinary pH in rabbit than in rat.

The difference in AE1 levels between the hyperacute Cl^--depletion alkalosis and the acute oral $NaHCO_3$ alkalosis of the present study suggests a possible two-stage response to acute alkali load. The first stage might consist of an initial kinetic down-regulation of AE1 function, though no such acute regulation of AE1 function in red cells or of anion exchange in Type A IC has yet been documented. The second, slower stage might be a decrease in AE1 polypeptide content, mediated by protein internalization and/or degradation. Operationally defined "degradation" of AE1 may result from epitope loss due to proteolysis, to conformational change, or to binding of another polypeptide. The cytoplasmic domains of erythroid and kidney isoforms of AE1 both undergo pH-dependent conformational changes [39, 40] that might contribute to epitope shielding. AE1 internalization might be modified by pH or by extracellular or intracellular $[K^+]$. Though plasma K^+ was not monitored in the current study, the $NaHCO_3$ alkalosis may have produced a mild hypokalemia. K^+ depletion inhibits assembly and endocytosis of clathrin-coated pits, though inhibition in fibroblasts required a 40% decrease in cell K^+ content [41]. In hyperacute Cl^--depletion alkalosis, intracellular K content of IC was indeed slightly reduced, though not to statistically significant levels [42]. Neither AE1 nor any other related AE polypeptide has yet been shown to localize to coated pits, or to associate with clathrin cage components. Moreover, inhibition of surface protein recycling ought not in the short term lead to a decrease in AE1 polypeptide content, but rather to an increase.

Altered transcription and stability of the AE1 mRNA could also contribute to regulation of AE1 polypeptide levels. In preliminary studies, Northern blot analysis of rat kidney cortex RNA pooled from three $NaHCO_3$ alkalotic animals showed a two- to threefold decrease compared to control (data not shown), consistent with an effect of alkalosis on AE1 mRNA synthesis and/or stability. Two previous studies have documented regulation of AE1 mRNA levels in renal cortex by chronic acid-base manipulations. Texeira da Silva et al [23] reported a two- to threefold increase in cortical AE1 mRNA levels after five days of respiratory acidosis imposed by a 10% CO_2 atmosphere. Fejes-Toth et al [14] examined isolated CCD cells and purified populations of Type A and Type B IC prepared from rabbits subjected to mineral acid or base loads 16 to 20 hours before sacrifice. They found an RT-PCR product of the AE1 gene was 4.5-fold more abundant in CCD cells from acidotic animals than from alkalotic animals. The difference was greater still in a cell fraction enriched for Type A IC, but the the study did not include control animals.

Fejes-Toth et al [14] also detected kidney AE1 polypeptide in rabbit CCD cell lysates, which increased in abundance in an acidotic animal. Our attempts to detect by immunoblot kidney AE1 in rat whole cortical lysates and various membrane fractions were prevented by proteolysis, which was considerably easier to block with inhibitors in membranes from mouse kidney than from rat kidney [35]. Taken together, however, our findings of decreased AE1 immunostaining intensity in acute alkalosis and increased staining intensity in acute acidosis are consistent with results of previous studies.

Our findings of H^+-ATPase localization alterations by acute metabolic acidosis and alkalosis are similar to earlier findings obtained with different experimental conditions. Verlander et al [26] reported ultrastructural evidence for redistribution of H^+-ATPase from the apical membrane to intracellular vesicles in Type A IC and its redistribution in Type B IC from intracellular vesicles to the basolateral membrane after two hours of acute metabolic alkalosis. The present findings in the CCD at four to six hours also resemble those reported after up to two weeks of metabolic alkalosis and acidosis by Bastani et al for rat kidney cortex H^+-ATPase [24].

The percentage of IC with apical H^+-ATPase staining in control, acidotic, and alkalotic states was lower in this work than those reported by Bastani et al, but the percentage of IC with apical/diffuse staining in this work was higher [24]. The increment in %IC which expressed apical H^+-ATPase in acidotic animals compared to control animals was much higher in the current study than after one day in the study of Bastani et al. The percentage of IC with basolateral H^+-ATPase staining was also lower in the current study. However, a nearly fourfold increase in the % of $AE1^-$ IC with basolateral H^+-ATPase was noted in alkalotic animals, a change not observed after 24 hours or less extreme alkalosis [24]. The low number of bipolar cells in the present study did not change with acidosis and alkalosis, in contrast to Bastani et al [24], who found bipolar cells reduced in acidosis and increased in chronic alkalosis.

The present analysis revealed a substantial population of Type A cells with apical H^+-ATPase staining that were negative for detectable AE1 staining. Up to 7.6% of IC in acidotic connecting segment fit this description. These may be cells with internalized AE1, as reported by the ultrastructural studies of Verlander et al [27, 31]. However, no "intravesicular" concentration of AE1 immunostaining was noted (at least at the light microscopic level), suggesting either proteolytic loss or shielding of the C-terminal epitope from primary antibody, rather than intracellular sequestration of AE1. Alternatively, these cells might represent a Type B IC variant in which the H^+-ATPase has moved to the apical

surface, or they may express a basolateral anion exchanger which is the product of another gene [43, 44].

Though acidosis and alkalosis produced dramatic changes in the intensity of AE1 immunostaining in the basolateral membrane of AE1-positive IC cells, the proportion of AE1-negative IC in CNT showed little change during acute metabolic acidosis or alkalosis (Tables 4 to 6). In CCD (Tables 7 to 9), this proportion decreased slightly with acidosis and increased slightly with alkalosis, but these changes did not achieve statistical significance. Four percent of IC were basolateral AE1-positive but lacked any H^+-ATPase immunostaining. This cell type, not previously reported, may have escaped previous detection [6] due to the smaller number of cells evaluated and/or the exclusive use of resin-embedded tissue. The cell may be a transitional intermediate, may have a distinct function, or could be an artifact of sectioning.

Functional consequences of acid/base perturbations in isolated perfused CCD from both rat and rabbit have been reported [1]. *In vivo* acid-loading led to decreased basolateral proton secretion by Type B cells in rabbit CCD [45], though regulation of rabbit CCD Type A IC function by *in vivo* acid loading has been found to be present [46] or absent [47, 48]. However, *in vitro* exposure of the isolated rabbit CCD to peritubular acidosis for as little as one hour was recently shown to reverse bicarbonate flux from net secretion to net absorption [49]. More recently, Narbaitz, Murugesan and Levine [50] reported that subacute (18 hr) acidosis in rats led to a slight increase in the % of IC which appeared by ultrastructural criteria to be of Type A, and to a doubling of the % of ultrastructurally defined "active" Type A IC. Most of these functional studies are consistent with the present immunocytochemical demonstration of regulation of AE1 levels and of H^+ ATPase localization.

The immunohistologically defined spectrum of IC in rat CCD is complex [24 and this work]. These and other published studies agree on the absence of AE1 epitopes in any IC apical membrane in intact kidney, though AE1 has been detected in apical membrane preparations of cultured rabbit Type B cells [13]. However, recent functional experiments suggest a more complex range of IC phenotypes than the classical Type A versus Type B categories. Isolated, perfused rabbit tubules show that all IC with apical Cl/HCO_3 exchange activity can also display basolateral Cl/HCO_3 exchange activity when assayed in specific ionic conditions [9, 10]. More recent data in both rat and mouse provide corroborating immunocytochemical evidence for the presence of non-AE1 AE anion exchanger epitopes in both apical and basolateral membranes of nearly all IC from control animals [43, 44]. Analyses of all these gene products during systemic and *ex vivo* acid/base manipulations will soon contribute to the next stage of our understanding of the remarkable plasticity of the collecting duct.

Acknowledgments

This work was supported by NIH grants DK43495 (SLA), DK42956 (DB) and by Fogarty International Research Grant (FIRCA) 1-RO3-TW00512 A-01-A1 (IS and DB). SLA is an Established Investigator of the American Heart Association. A portion of this work was presented at the 24th annual meeting of the American Society of Nephrology (*J Am Soc Nephrol* 2:693, 1991). We thank Robert Tyszkowski, John Lydon, Gary Lloyd, and Alan Stuart-Tilley for technical and graphics assistance.

Reprint requests to Seth L. Alper, M.D., Molecular Medicine Unit, Beth Israel Hospital, 330 Brookline Ave., Boston, Massachusetts 02215, USA.

E-mail: salper@bih.harvard.edu

Appendix

Abbreviations are: IC, intercalated cells; CCD, cortical collecting duct; CNT, connecting segment; PLP, paraformaldehyde/lysine/periodate; PC, principal cells; PBS, phosphate-buffered saline.

References

1. Schuster VL: Function and regulation of intercalated cells. *Annu Rev Physiol* 55:267–288, 1993
2. Drenckhahn D, Schluter K, Allen DP, Bennett V: Colocalization of band 3 with ankyrin and spectrin at the basal membrane of intercalated cells in the rat kidney. *Science* 230:1287–1289, 1985
3. Schuster VL, Bonsib SM, Jennings ML: Two types of collecting duct mitochondria-rich (intercalated) cells: Lectin and band 3 cytochemistry. *Am J Physiol* 251:C347–C355, 1986
4. Verlander, JW, Madsen KM, Low PS, Allen DP, Tisher CC: Immunocytochemical localization of band 3protein in the rat collecting duct. *Am J Physiol* 255:F115–F125, 1988
5. Brown D, Hirsch S, Gluck S: An H^+-ATPase is present in opposite plasma membrane domains in subpopulations of kidney epithelial cells. *Nature* 331:622–624, 1988
6. Alper SL, Natale J, Gluck S, Lodish HF, Brown D: Subtypes of intercalated cells in rat kidney collecting duct defined by antibodies against erythroid band 3 and renal vacuolar H^+-ATPase. *Proc Natl Acad Sci USA* 86:5429–5433, 1989
7. Schuster VL, Fejes-Toth G, Naray-Fejes-Toth A, Gluck S: Colocalization of H(+)-ATPase and band 3 anion exchanger in rabbit collecting duct intercalated cells. *Am J Physiol* 260:F506–F517, 1991
8. Hayashi M, Yamaji Y, Iyori M, Kitajima W, Saruta T: Effect of isoproterenol on intracellular pH of the intercalated cells in the rabbit cortical collecting ducts. *J Clin Invest* 87:1153–1157, 1991
9. Weiner ID, Weill AE, New AR: Distribution of Cl/HCO_3 exchange and intercalated cells in rabbit cortical collecting duct. *Am J Physiol* 267:F952–F964, 1994
10. Emmons C, Kurtz I: Functional characterization of three intercalated cell subtypes in the rabbit outer cortical collecting duct. *J Clin Invest* 93:417–423, 1994
11. Wingo CS, Cain BD: The renal H-K-ATPase: Physiological significance and role in potassium homeostasis. *Annu Rev Physiol* 55:323–347, 1993
12. Alper SL: The band 3-related AE anion exchanger gene family. *Cell Physiol Biochem* 4:265–281, 1994
13. van Adelsberg J, Edwards JC, Al-Awqati Q: The apical Cl/HCO_3 exchanger of β intercalated cells. *J Biol Chem* 268:11283–11289, 1993
14. Fejes-Toth G, Chen W-R, Rusvai E, Moser T, Naray-Fejes-Toth A: Differential expression of AE1 in renal HCO_3-secreting and -reabsorbing intercalated cells. *J Biol Chem* 269:26717–26721, 1994
15. Breton S, Alper SL, Gluck SL, Sly WS, Barker J, Brown D: Depletion of intercalated cells in collecting ducts of carbonic anhydrase II-deficient (CAR2) mice. *Am J Physiol (Renal)* 269:F761–F774, 1995
16. Teng-umnuay P, Verlander JW, Yuan W, Tisher CC, Madsen K: Identification of distinct subpopulations of intercalated cells in the mouse collecting duct. *J Am Soc Nephrol* 7:260–274
17. Cox KH, Cox JV: Variant chicken AE1 anion exchangers possess divergent NH2-terminal cytoplasmic domains. *Am J Physiol (Renal)* 268:F503–F513, 1995
18. Wagner S, Vogel R, Lewitzke R, Koob R, Drenckhahn D: Immunochemical characterization of a band 3-like anion exchanger in collecting duct of human kidney. *Am J Physiol (Renal)* 253:F213–F221, 1987
19. Drenckhahn D, Oelmann M, Schaaf P, Wagner M, Wagner S: Band 3 is the basolateral anion exchanger of the dark epithelial cells of the turtle urinary bladder. *Am J Physiol (Cell)* 252:C570–C574, 1987
20. Brosius FC, Alper SL, Garcia AM, Lodish HF: The major kidney band 3 gene transcript predicts an amino-terminal truncated band 3 polypeptide. *J Biol Chem* 264:7784–7787, 1989

21. KUDRYCKI KE, SHULL GE: Primary structure of the rat kidney band 3 anion exchange protein deduced from a cDNA. *J Biol Chem* 264:8185–8192, 1989
22. KOLLERT-JONS A, WAGNER S, HUBNER S, APPELHANS H, DRENCKHAHN D: Anion exchanger 1 in human kidney and oncocytoma differs from erythroid AE1 in its NH_2 terminus. *Am J Physiol (Renal)* 265:F813–F821, 1993
23. TEXEIRA DA SILVA JCJ, PERRONE RD, JOHNS CA, MADIAS NE: Rat kidney band 3 mRNA modulation in chronic respiratory acidosis. *Am J Physiol* 260:F204–F209, 1991
24. BASTANI B, PURCELL H, HEMKEN P, TRIGG D, GLUCK S: Expression and distribution of renal vacuolar proton-translocating adenosine triphosphatase in response to chronic acid and alkali loads in the rat. *J Clin Invest* 88:126–136, 1991
25. PURCELL H, BASTANI B, HARRIS KP, HEMKEN P, KLAHR S, GLUCK S: Cellular distribution of H(+)-ATPase following acute unilateral ureteral obstruction in rats. *Am J Physiol* 261:F365–F376, 1991
26. VERLANDER JW, MADSEN KM, GALLA JH, LUKE RG, TISHER CC: Response of intercalated cells to chloride depletion metabolic alkalosis. *Am J Physiol* 262:F309–F319, 1992
27. KIM J, WELCH WJ, CANNON JK, TISHER CC, MADSEN KM: Immunocytochemical response of type A and type B intercalated cells to increased sodium chloride delivery. *Am J Physiol* 262:F288–F302, 1992
28. NARBAITZ R, KAPAI VK, LEVINE DZ: Induction of intercalated cell changes in rat pups from acid- and alkali-loaded mothers. *Am J Physiol* 264:F415–F420, 1993
29. BROWN D, GLUCK S, HARTWIG J: Structure of the novel membrane-coating in proton-secreting epithelial cells and identification as an H^+-ATPase. *J Cell Biol* 105:1637–1648, 1987
30. MADSEN KM, KIM J, TISHER CC: Intracellular band 3 immunostaining in type A intercalated cells of rabbit kidney. *Am J Physiol* 262:F1015–F1022, 1992
31. VERLANDER JW, MADSEN KM, CANNON JK, TISHER CC: Activation of acid-secreting intercalated cells in rabbit collecting duct with ammonium chloride loading. *Am J Physiol* 266:F633–F645, 1994
32. GIFFORD JD, SHARKINS K, WORK J, LUKE RG, GALLA JH: Total CO_2 transport in rat cortical collecting duct in chloride-depletion alkalosis. *Am J Physiol* 258:F848–F853, 1990
33. BROWN D, HIRSCH S, GLUCK S: Localization of H^+-ATPase in rat kidney. *J Clin Invest* 82:2114–2126, 1988
34. ALPER SL, STUART-TILLEY A, SIMMONS CF, BROWN D, DRENCKHAHN D: The fodrin-ankyrin cytoskeleton of choroid plexus preferentially colocalizes with apical Na^+,K^+-ATPase rather than with basolateral anion exchanger AE2. *J Clin Invest* 93:1430–1438, 1994
35. BROSIUS FC, NGUYEN K, STUART-TILLEY AK, HALLER C, BRIGGS JP, ALPER SL: Regional and segmental localization of AE2 anion exchanger mRNA and protein in rat kidney. *Am J Physiol* 269:F461–F468, 1995
36. BROWN D, SABOLIC I: Endosomal pathways for water channel and proton pump recycling in kidney epithelial cells. *J Cell Sci* 17(Suppl): 49–59, 1993
37. EMMONS C: The majority of rat outer CCD intercalated cells have either basolateral or both apical and basolateral Na^+-independent Cl/base exchangers. (abstract) *J Am Soc Nephrol* 3:776, 1993
38. SCHWARTZ GJ, BARASCH J, AL-AWQATI Q: Plasticity of epithelial polarity. *Nature* 318:368–371, 1995
39. BICKNESE S, ROSSI M, THEVENIN B, SHOHET SB, VERKMAN AS: Anisotropy decay measurement of segmental dynamics of the anion binding domain in erythrocyte band 3. *Biochemistry* 34:10645–10651, 1995
40. WANG CC, MORIYAMA R, LOMBARDO CR, LOW PS: Partial characterization of the cytoplasmic domain of human kidney band 3. *J Biol Chem* 270:17892–17897, 1995
41. LARKIN JM, BROWN MS, GOLDSTEIN JL, ANDERSON RG: Depletion of intracellular potassium arrests coated pit formation and receptor-mediated endocytosis in fibroblasts. *Cell* 33:273–285, 1983
42. GIFFORD JD, GALLA JH, LUKE RG, RICK R: Ion concentrations in the rat CCD: Differences in cell types and effect of alkalosis. *Am J Physiol* 259:F778–F782, 1990
43. ALPER SL, STUART-TILLEY AK, BROWN D: Immunolocalization of AE2 anion exchanger in rat kidney. (abstract) *J Am Soc Nephrol* 6:371, 1995
44. ALPER SL, STUART-TILLEY AK, YANNOUKAKOS D, BROWN D: AE3 anion exchanger immunolocalization in rodent kidney: Evidence for apical and basolateral isoforms. (abstract) *J Am Soc Nephrol* 6:372, 1995
45. YAMAJI Y, HAYASHI M, IYORI M, SARUTA T: Pertubular metabolic acidosis decreases H^+-pump activity of b intercalated cell. (abstract) *J Am Soc Nephrol* 2:717, 1991
46. ISHIBASHI K, SASAKI S, YOSHIYAMA N, SHIIGAI T, TAKEUCHI J: Generation of pH gradient across the rabbit collecting duct segments perfused in vitro. *Kidney Int* 31:930–936, 1987
47. GARCIA-AUSTT J, GODD DW, BURG M, KNEPPER MA: Deoxycorticosterone-stimulated bicarbonate secretion in rabbit cortical collecting ducts: Effects of luminal chloride removal and in vivo acid loading. *Am J Physiol* 249:F205–F212, 1985
48. HAMM LL, HERING-SMITH KS, VEHASKARI VM: Control bicarbonate transport in collecting tublues from normal and remnant kidneys. *Am J Physiol* 256:F680–F687, 1989
49. TSURUOKA S, SCHWARTZ GJ: Adaptation of rabbit cortical collecting duct HCO_3-transport to metabolic acidosis in vitro. *J Clin Invest* 97:1076–1084, 1996
50. NARBAITZ R, MURUGESAN S, LEVINE DZ: K depletion and NH_4Cl acidosis increase apical insertion of studded membrane in type A-intercalated cells. *Am J Physiol* 270:F649–F656, 1996